In-plane and out-of-plane testing of masonry walls strengthened using polymer textile reinforced mortar

Najif Ismail[a]
[a]Assistant Professor, Department of Civil and Environmental Engineering, United Arab Emirates University, PO Box 15551, Al Ain 1818, United Arab Emirates; najif@uaeu.ac.ae

Jason M. Ingham[b]
[b]Professor, Department of Civil and Environmental Engineering, University of Auckland, Private Bag 92019, Auckland 1142, New Zealand; j.ingham@auckland.ac.nz

Abstract

Details of an experimental program investigating the structural performance of unreinforced masonry (URM) walls strengthened using two different types of polymer textile reinforced mortar (TRM) is presented. The experimental program involved full scale reversed cyclic in-plane and out-of-plane testing of TRM strengthened URM walls. The testing was performed in two series, with series 1 involving in-plane testing of three (03) pier-spandrel assemblages representing part of a perforated URM wall and series 2 involving out-of-plane testing of three (03) slender walls having no penetrations. To replicate the physical characteristics of historic masonry materials, vintage solid clay bricks and a low strength hydraulic cement mortar were used for construction of the test walls. Numerous structural characteristics pertaining to the seismic behaviour of TRM strengthened historic URM walls were investigated and then compared to those obtained from corresponding as-built tested URM walls. In general, strengthened walls exhibited a ductile behaviour until the polymer textile ruptured in a brittle manner. The strength increment due to TRM strengthening was observed to range from 128% to 136% when the URM test walls were loaded in-plane and from 575% to 786% when the URM test walls were loaded out-of-plane. TRM strengthening also resulted in a

notable increment in deformation capacity and ductility of strengthened test walls.

Keywords: seismic strengthening; structural testing; in-plane; out-of-plane; brick masonry; polymeric composites; polymer textile.

1. Introduction

Unreinforced masonry load bearing (URM) walls have routinely been documented to exhibit poor seismic performance during moderate to severe earthquakes, resulting in partial or complete collapse of the building [1-5]. The observed poor seismic performance of URM buildings has highlighted the seismic hazard associated with this form of construction, and the need for further investigation to advance the understanding of aspects related to their seismic assessment and improvement.

In the event of an earthquake, gravity loaded URM walls are also subjected to lateral loading either oriented parallel (referred to as in-plane load actions) or oriented perpendicular (referred to as out-of-plane load actions) with respect to their stronger plane, or the URM wall may be subjected to a combination of both lateral load actions. The seismic behaviour of in-plane loaded perforated URM walls (also referred to as URM equivalent frames) is explained by delineating these walls into separate spandrel, joint, and pier elements. Spandrels and piers have been observed to undergo damage more frequently than the joint regions [6], with the failure of pier and spandrel elements being either flexural controlled or shear controlled (or a combination of both). The flexural controlled failure mode is characterised by horizontal cracking at pier tops and bases, flexural vertical cracks at pier-spandrel interfaces, and/or compression crushing at plastic hinge locations (i.e. toe region of piers) that results due to rocking of piers. Sliding along a mortar joint (step joint or bed joint) or diagonal cracking through bricks [7], in either spandrels

or piers, are the two most frequently noted shear controlled failure modes in URM frames. Out-of-plane loaded slender URM walls typically undergo partial or complete out-of-plane collapse during moderate to severe earthquakes, which can result due to flexural failure of the wall and/or wall anchorage failure [8]. Assuming the presence of adequate wall-diaphragm anchorages to provide sufficient lateral restraint, out-of-plane loading causes bending in the URM wall and depending upon the specifics of the boundary restraints leads to either one-way or two-way bending. Typically, slender historic URM walls with height to thickness ratios greater than 14 are prone to out-of-plane failure when deforming in a one way bending mode [9, 10].

A number of seismic strengthening techniques have been implemented in the past to improve the seismic performance of URM buildings. Of these, fibre reinforced polymers (FRP) have attracted notable interest from academia and practicing engineers for application to the seismic retrofit of URM buildings owing to their high strength to weight ratio, thinner cross-sections, non-corrosive nature of constituent materials, and the ease of application [11-15]. Typical polymer-based seismic retrofit solutions involve full overlay of epoxy impregnated FRP sheets onto the surface of URM walls, surface bonding of polymer plates using epoxy, and near surface mounting of polymer strips/bars. However, the technical literature also suggests several challenges/disadvantages associated with the use of organic epoxies in such FRP application [16]. Amongst these disadvantages are their irreversible nature, stiffness incompatibility with historic URM materials, vapour impermeability, and poor performance both at elevated temperatures (typically higher than 60–80°C) and in alkaline environments [17].

One alternative to overcome these challenges is the use of inorganic cementitious matrices to bond semi-finished or pre-primed dry grid pattern external FRP fabrics, which is typically referred to as a polymer grid pattern polymer textile reinforced mortar (TRM). The

TRM strengthening technique is relatively new and is deemed to have several advantages over its counterpart epoxy impregnated FRP overlay, including stiffness compatibility with historic URM materials, flexibility to bend without failure that allows its application over curved surfaces, and relatively higher resistance to elevated temperature and alkali attack, minimal handling problems, and the ability to create a water resistant but vapour permeable layer [18]. However, there exists a paucity of experimental results available in technical literature on the effectiveness of TRM for seismic strengthening and repairing of perforated URM walls, which motivated the experimental study reported herein.

An experimental program involving full scale reversed cyclic in-plane and out-of-plane testing of TRM strengthened URM walls with realistic test boundary conditions was undertaken and numerous parameters pertaining to their seismic performance were investigated. It is noted that the combined effect of in-plane and out-of-plane loading was not investigated. The experimental results from TRM strengthened/repaired test walls were then compared to that from a corresponding as-built test wall and structural improvements in terms of stiffness, strength, ductility, and damping properties were commented on. The experimental results provide proof of the design concept of a relatively new strengthening and repairing system.

2.1. Past testing and design guidelines

A number of experimental programs were previously undertaken to investigate the effectiveness of TRM for seismic strengthening of reinforced concrete structural elements [14, 18-22]. Experimental studies have also investigated the effectiveness of TRM systems for restraining the diagonal shear cracking of in-plane loaded URM walls/panels [22-25]. Almieda et al. [26] undertook cyclic shear testing of as built and TRM strengthened URM wallettes and

reported the shear strength of TRM strengthened wallettes to be 2.3 times that of as-built URM wallettes. However, quasi-static cyclic testing of full scale as-built URM frame assemblies [27-30] showed that the URM frames exhibit complex behaviour and that the results obtained from testing of individual panels do not accurately represent the seismic behaviour of perforated URM walls. To this end, Augenti et al. [31] performed quasi-static testing of a single perforated URM wall, which was first tested as-built and then repaired using a TRM system. It was concluded that the repair using TRM not only restored the in-plane strength, but also increased the ductility capacity of the wall. The test results from the same set of experiments were then used to develop a nonlinear model to estimate the strength of TRM strengthened URM walls [32].

The cyclic out-of-plane flexural response of small scale TRM retrofitted masonry assemblages has been investigated by performing pseudo-static cyclic out-of-plane testing [33, 34], with loading being applied using a three point loading arrangement. Following the above mentioned experimental studies it was reported that TRM is a viable seismic retrofit technique for masonry walls, and a large strength increment was reported for retrofitted masonry assemblages when compared to corresponding as-built tested masonry assemblages. Babaeidarabad et al. [35] performed out-of-plane testing of nine scaled URM walls using an air bag based test setup, of these 3 were tested as-built and six were strengthened by applying full overlay of TRM on both faces. It was reported that the flexural strength of the TRM specimens ranged between 2.8 and 7.5 times that of the control URM walls, depending upon the number of grid layers used. The research led to the publication of the guidelines for the design of TRM strengthening intervention for concrete and URM buildings [16].

2. Experimental Program

The experimental program was comprised of two series of tests. Series 1 involved pseudo-static reversed cyclic in-plane testing of three (03) TRM strengthened full scale pier-spandrel assemblages (representing part of a perforated URM wall, also referred to as a URM frame) and series 2 involved reversed cyclic out-of-plane testing of three (03) full scale slender URM walls. Series 2 testing was further performed in two stages, with the first stage involving the testing of walls subjected to reversed cyclic loading up to a drift of roughly 4% and the second stage of testing involving walls loaded in one direction only until the wall collapsed. Because the majority of heritage URM buildings have exposed brickwork on their exterior façade and therefore a strengthening application is only desirable on the interior wall face, the experimental program considered only one sided TRM strengthening, as is the norm for earthquake strengthening of historic URM buildings.

2.1. Wall specifications

Test wall dimensions and strengthening details are shown in Table 1. Test walls were given the notation ABX-N or TMX-N, where AB refers to as-built tested walls, TM refers to test walls strengthened using TRM, X denotes the loading direction (I refers to in-plane and O refers to out-of-plane) and N denotes the test number. It should be noted that test assemblage ABI-1 was tested as-built and subsequently repaired by repointing the spandrel cracks and having a single sided TRM full surface overlay applied on the spandrel (the repaired assemblage is referred to as test assemblage TMI-2). Because the piers of assemblage TMI-2 were completely intact at the conclusion of testing, for the construction of test assemblage TMI-3 the existing piers were reused and a new spandrel was reconstructed.

Figure 1a shows the geometric dimensions of series 1 pier-spandrel assemblages. The test assemblages were constructed over two concrete footings, which were anchored to the laboratory strong floor to avoid lateral sliding of the piers but allow bed joint shear sliding to potentially occur at the pier base. It was observed in previously performed testing of such as-built pier-spandrel URM assemblages [17] that damage was mostly concentrated in the unsupported middle span of the spandrels. Therefore, to limit such damage, the spandrel of both test assemblages was strengthened by applying a full TRM overlay on one face and the piers were left unstrengthened. Figure 1b shows the geometric dimensions of series 2 test walls, which were strengthened by applying a full TRM overlay on one face.

2.2. Material properties

All test walls were constructed by an experienced brick layer under supervision. The masonry was laid following a common bond pattern, with roughly 15 mm thick mortar bed joints between two successive brick courses. Lumantarna et al. [36] investigated the physical and chemical characteristics of historic mortar prevalent in New Zealand URM buildings by testing mortar samples extracted from a number of URM buildings located across New Zealand and suggested that a volumetric cement:lime:sand ratio of 1:2:9 closely replicate the physical characteristics of mortar prevalent in historic New Zealand URM buildings. Therefore, the same mortar composition was used to construct the test walls. Vintage solid clay bricks used to construct the test walls were approximately 100 years old, being 220 mm long × 110 mm wide × 75 mm high and recycled from the rubble of two different historical URM buildings (one source for each series of testing).

Physical characteristics of the constituent masonry materials were determined using

standardised testing procedures. Masonry flexural bond strength was determined by testing masonry prisms in accordance with ASTM C1072-10 [37]. Mortar compressive strength was determined by testing 50 mm mortar cubes in accordance with ASTM C109-11 [38]. The compressive strength of bricks and masonry were determined in accordance with ASTM C67-11 [39] and ASTM C1314-11 [40] respectively. The test results are reported in Table 2 as mean values and corresponding coefficients of variation (COV). Two different types of commercially available TRM systems were selected for based on the results of material testing performed as part of this study and on the results of a precedent study [24] that involved diagonal shear testing of URM wallettes in accordance with ASTM E519-10 [41], which were strengthened using both single sided and double sided overlays of a variety of commercially available TRM systems. Tensile testing of polymer fabric and adhesion of TRM system used were determined experimentally in accordance with ASTM C321-00 [42] ASTM D7269-11 [43], respectively. Indicative mechanical characteristic of the used strengthening materials are also reported in Table 3.

2.3. Strengthening procedure

The masonry surface that was to receive seismic strengthening was first prepared by removing all disintegrated masonry fragments, dust, oil and paintwork. The cleaned substrate was made wet by sprinkling water and was then left to dry until a saturated surface dry (SSD) condition was achieved. As the masonry surface was uneven, a levelling mortar layer being 5-15 mm thick was applied over the cleaned SSD masonry surface. In test walls TMI-03 and TMO-06 an additional galvanised steel mesh was fixed using 100 mm long light capacity steel mechanical anchor assemblies, to avoid TRM de-bonding. To install these steel anchors, dowel sleeves were inserted into equally spaced pre-drilled holes (roughly 300 mm o.c. in both directions). The steel

mesh was placed between the retaining discs and the steel anchors were driven into the dowel sleeves. The levelling mortar layer was then left to cure for three days until it was completely dry. A 3-4 mm thick layer of a commercial adhesive mortar was uniformly applied over the dry levelling mortar layer using a flat metal trowel. The textile was pressed into the freshly applied adhesive mortar layer so that mortar protruded through the textile grid openings. Finally, a 2-3 mm thick rendering coat of adhesive mortar was applied. The recommended curing time for commercially available adhesive mortars for such TRM strengthening applications varies between 7 to 28 days.

2.3.1. Series 1 testing details

A gradually increasing displacement controlled reversed cyclic loading history was applied at the topmost fibre of series 1 test assemblages using a rigid steel loading beam, with each displacement excursion repeated twice. The displacement was increased as a function of drift values, with an increment step of 0.2% drift between two consecutive excursions. The testing of strengthened assemblages was continued until either the hydraulic ram reached its stroke capacity or the post-peak strength of the assemblage degraded to 80% of the peak strength. The reversed cyclic pseudo-static lateral loading was applied using a hydraulic ram coupled with a 500 kN load cell, which were together positioned between the loading beam and the strong wall. The loading beam was supported on top of the spandrel by two sets of rollers, with these rollers positioned at the centreline of each pier. The rollers minimized frictional resistance between the loading beam and the test assemblage. An axial force of 44 kN was applied to each pier using two external posttensioned (PT) threaded bars, replicating the overburden weight as if the test assemblages were located at the lower storey of a two storey URM building. The magnitude of applied axial load was maintained by placing a spring at the

bottom of each PT tendon, between the strong floor and the end anchorage plates. Additionally, PT tendon stress variation was monitored by placing a 40 kN load cell at the top end of each PT bar. A total of 34 portal gauges were used to record deformations in the piers and the spandrel and two control displacement gauges (Z1 and Z2) were attached to the spandrel at one end and to a free standing steel frame at the other end. Figure 2 shows the test setup used for series 1 testing, where LC refers to load cell; P refers to pier (suffix A and B identify the pier location); S refers to spandrel; H refers to horizontal; V refers to vertical; X refers to diagonal; PC refers to pier-spandrel connection; B refers to pier base; and Z refers to control displacement gauges recording the lateral displacement.

2.3.2. Series 2 testing details

Reversed cyclic out-of-plane testing was performed using the test setup shown in Figure 3a, being consistent with similar precedent research studies [44, 45]. In the first stage of testing a pair of air bags was positioned on each side of the wall between the test wall and a backing frame to apply a uniformly distributed pseudo-static load. The backing frames were placed over two pairs of smooth greased steel plates having negligible friction, such that the backing frame self-weight did not impair the test results. One linear variable differential transducer (LVDT) was located at wall mid-height to determine lateral displacement and eight 10 kN s-shape load cells (with four on each side of the wall) were used to determine the magnitude of applied lateral force. The strong reaction frame acted as a backing and also supported the top of the wall, creating boundary conditions that were comparable to those when a strengthened wall is connected to a floor or ceiling diaphragm. Gradually increasing displacement controlled cyclic loading was applied by alternatively inflating and deflating the air bags. Displacement amplitude for every third loading cycle was increased gradually as a function

of wall drift, with each displacement cycle consisting of a push and pull excursion. The reversed cyclic testing was continued until the test came into contact with the backing frames. Therefore, in the second stage of testing, one backing frame was removed and the strengthened walls were tested up to collapse by applying one-directional cyclic loading (refer to Figure 3b). This loading arrangement enabled the behaviour of TRM strengthened URM walls to be established when loaded out-of-plane to beyond the collapse prevention limit state, which is not well documented in technical literature.

3. Experimental Results and Discussion

An overview of testing results is reported in Table 4. The first cracking limit state corresponds to the elastic limit of the test walls, which was observed to occur at an applied lateral force of approximately $0.7V_u$ and is consistent with typical code recommended elastic limits for a bi-linear idealisation [9, 46]. The ultimate strength limit state was defined as the point on the experimental force-displacement curves when post-peak strength degraded to 80% of the peak strength. Ductility was quantified using the measured ultimate drift ratio, calculated as $\gamma_u = \frac{\Delta_u}{H}$ for in-plane loaded walls and as $\gamma_u = \frac{2\Delta_u}{H}$ for out-of-plane loaded walls, where Δ_u is the lateral displacement corresponding to an ultimate strength limit state and H is the effective height of the wall. Additionally, a pseudo-ductility value $\mu = \frac{\Delta_u}{\Delta_y}$ was calculated for each test wall, where Δ_y is the effective yield displacement corresponding to extrapolation of the first cracking limit state when considering a bi-linear elasto-plastic system (refer Figure 4). It should be noted that as the bi-directional cyclic testing was stopped before the walls reached their ultimate strength limit state, the maximum measured drift values determined for test walls ABO-

4, TMO-5 and TMO-6 give conservative ultimate drift values.

3.1. Failure modes

3.1.1. Series 1 testing

Figures 5 shows damage patterns observed at the conclusion of series 1 testing. The as-built tested wall ABI-1 exhibited a strong-pier weak-beam failure mechanism, with pier rocking resulting in opening of horizontal cracks at the base of each pier and diagonal shear cracks forming in the middle portion of the spandrel. Some localised cracking was also observed at the projecting edges of the spandrel, which was attributed to stress concentration at the interface between the masonry and the edge of the loading beam. The damage pattern observed for test wall TMI-2 was similar to that for as-built tested wall ABI-1, being rocking induced cracking in the middle portion of the spandrel. The majority of cracks were observed to propagate through mortar joints, which were attributed to the low ratio of mortar strength to brick strength. A horizontal bed joint crack at the unstrengthened spandrel-pier connection was also observed to widen before the textile rovings that crossed the spandrel cracks started to rupture and resulted in rapid loss of wall strength.

Test wall TMI-3 also exhibited pier rocking until one of the piers failed in a step joint sliding shear failure mode, without any visible cracking in the spandrel. It was established from the failure mode observed for TMI-3 that careful consideration was necessary regarding to the amount of strength increase applied to the spandrel, with respect to the assessed pier strength, in order to avoid such brittle shear failure of the piers. Alternatively to avoid pier diagonal shear failure, TRM strengthening of URM piers at selected locations could also be performed, such that the strength corresponding to all three possible failure modes (pier cracking, spandrel

cracking and cracking at the spandrel-pier connection) is greater than the seismic demand corresponding to a moderate earthquake and in the event of a large magnitude earthquake the spandrel-pier connection fails before either of the piers or the spandrel reaches ultimate strength.

3.1.2. Series 2 testing

Figure 6 shows the damage patterns observed at the conclusion of stage 1 and stage 2 of series 2 testing. The as-built tested wall ABO-4 behaved linearly until a single large horizontal crack developed at a location that was three courses above wall mid-height, separating the wall into two portions. Upon further application of lateral out-of-plane loading, the upper and the lower portions of the wall started to rock about the crack location and continued to exhibit this rocking phenomenon until the test was stopped prior to reaching an instability mid-height displacement. In test walls TMO-5 and TMO-6, when subjected to face loading causing compression stresses in the TRM layer, a horizontal crack developed near the top end of the wall, that started to widen upon further application of face loading in the same direction. When the strengthened walls were subjected to face loading in the opposite direction, the textile reinforcement acted in tension and distributed stresses over a large masonry area, resulting in several hairline horizontal cracks to form on the TRM surface.

The second stage of series 2 testing was continued until the walls collapsed. Test wall TMO-5′ continued to resist the applied loading, with opening of several distributed hairline flexural cracks until rupture of the polymeric textile rovings that crossed a single bed joint crack located near mid-height (refer Figure 7a), resulting in sudden wall collapse. Test wall TMO-6′ exhibited a similar failure mode but the additional steel mesh reinforcement provided some lateral resistance even after the polymeric textile reached its ultimate capacity, thus avoiding collapse of the test wall (refer Figure 7b).

3.2. Force-displacement response

Figures 8a to 8f show the measured hysteretic response for the test walls, with secondary axes to allow comparison of experimental results for walls of different height. The secondary horizontal axis represents drift values, calculated as $\gamma = \frac{\Delta}{H}$ for in-plane loaded walls and as $\gamma = \frac{2\Delta}{H}$ for out-of-plane loaded walls, where Δ is the lateral displacement and H is the wall/assemblage height. Additionally, analogous moment values are shown on the secondary vertical axis for out-of-plane loaded walls, calculated as $M = \frac{VH}{8}$ where V is the total applied lateral force and H is the wall height. The result for the corresponding as-built tested wall (dotted line) is also included on each plot, to illustrate the seismic improvement due to TRM strengthening.

3.2.1. Series 1 testing

The as-built tested wall ABI-1 responded linearly until cracking occurred in the spandrel, resulting in narrow hysteretic loops which are typical for psueudo-statically rocking structures where no account is made for radiation damping due to dynamic rocking. The test wall did not exhibit any loss of strength and continued to resist lateral force even at large displacement excursions until the hydraulic ram reached its stroke capacity and the testing could not be continued further.In test wall TMI-2, the TRM layer resisted crack openings by distributing stresses over a large masonry area until textile rovings spanning across cracks started to rupture at a lateral displacement of 38.5 mm. As a result the repaired wall TMI-2 exhibited larger energy dissipation than the as-built tested wall ABI-1, resulting in larger hysteretic loops. The

strengthened test wall TMI-3 exhibited a rocking response and resulted in relatively pinched hysteretic loops. The strengthened spandrel of TMI-3 did not reach its cracking strength before one pier failed in diagonal shear at a lateral displacement of 36.8 mm, which led to rapid post-peak wall strength loss. Figure 8g shows the comparison between the maximum excursion curves of series 1 walls.

3.2.2. Series 2 testing

For the bi-directional cyclic testing (ABO-4, TMO-5 and TMO-6), testing of all walls was discontinued prior to reaching ultimate strength and post-peak strength was not observed for any of the test walls, as shown in the experimental force-displacement plots. The as-built tested wall ABO-4 behaved linearly up to cracking and then started to exhibit rigid body rocking without further strength gain. Test walls TMO-5 and TMO-6 exhibited a bi-linear response, with both walls having minor flexural cracking and returning to their original positions without any residual displacement. The flexural strength of these walls was observed to be noteably higher than for the as-built wall ABO-4 when the TRM layer acted in tension, but when the walls were loaded in the reverse direction and the TRM acted in compression, the strengthened walls performed similarly to the as-built test wall ABO-4. The observed asymmetric strength increment for single sided strengthened walls suggested that a two sided TRM strengthening strategy should be performed for URM walls, which could either be applied as a full surface overlay or as vertical strips offset on each side of the wall.

In the second stage of testing, strengthened walls TMO-5′ and TMO-6′ continued to exhibit a bi-linear behaviour, similar to that observed in the first stage, until the tensile strength of the reinforcement textile was exceeded and the walls collapsed. Figure 8h shows the comparison between the maximum excursion curves for series 2 walls. In general, the

strengthened walls exhibited similar behaviour, with the governing failure mode being brittle and the ultimate strength of the walls dictated by the tensile strength of the polymer textile. Test wall TMO-6′ performed relatively better than test wall TMO-5′ and failed at a larger out-of-plane force in a relatively more ductile failure mode, which was partially attributed to the introduction of additional steel mesh.

3.3. Stiffness degradation and energy dissipation

To quantify stiffness degradation that occurred in each test wall, the wall secant stiffness for each loading cycle was determined as the secant modulus between the maximum excursion points of a hysteretic loop (see Figure 4). The determined wall secant stiffness is plotted in Figures 9a and 9c against the displacement amplitude of the corresponding loading cycle. The energy dissipated in each cycle was determined by integrating the area bounded by the loading and unloading curves of each loop and the cumulative dissipated energy is plotted in Figures 9b and 9d. Equivalent hysteretic damping coefficients were calculated from experimental results using Equation 1 proposed by Chopra [47], where ξ = damping coefficient; E_D = area between loading and unloading curve; and E_{SO} = area of right angle triangle with perpendicular equal to maximum force and base equal to corresponding displacement. The calculated equivalent viscous damping coefficients for the first cycle were also reported in Table 4.

$$\zeta = \frac{E_D}{2\pi\pi_{SO}} \quad (1)$$

4. Summary and Conclusions

The history and development of TRM systems is briefly discussed. A summary of precedent experimental programs was presented, with regard to repair and strengthening of masonry structures and a gap in the current technical literature was identified. An overview was

provided of an experimental program that was undertaken to investigate the performance of URM walls strengthened using TRM. The experimental program consisted of several small scale standardised material tests, pseudo-static reverse cyclic testing of three large scale TRM strengthened URM assemblages (series 1), and out-of-plane flexural testing of three full scale slender URM walls (series 2). Two commercially available TRM systems, selected on the basis of a precedent study, were used to strengthen the test walls. Numerous structural characteristics pertaining to the seismic behaviour of TRM strengthened historic URM walls were investigated and then compared to those obtained from as-built tested URM walls. The key findings of the experimental program are:

- In general, the two TRM systems performed similarly and resulted in similar strength increments. However, the introduction of steel mesh in addition to the TRM resulted in a small increase in the strength and ductility of the test walls.

- The primary reinforcement mechanism for TRM systems is the distribution of stresses over a large area prior to masonry cracking and once the masonry began to crack (micro hairline cracking), the textile rovings spanning these cracks acted in tension to resist further opening of these cracks.

- The in-plane strength of pier-spandrel assemblages having a TRM strengthened spandrel ranged from 128% to 136% when compared to their as-built strength.

- Two different failure modes were observed for in-plane loaded strengthened pier-spandrel assemblages, the first being the rupture of textile rovings spanning masonry cracks and the second being shear failure of unstrengthened piers without any spandrel cracking.

- It was established that in-plane loaded URM pier-spandrel assemblages should be strengthened at selected locations, with a strengthening scheme selected such that the strength corresponding to all three possible failure modes (pier cracking, spandrel cracking and cracking at the spandrel-pier connection) is greater than the strength demand corresponding to a moderate earthquake and that in the event of a large magnitude earthquake the spandrel-pier connection fails before either of the piers or the spandrel reach their ultimate shear/flexural capacity, such that a pier rocking mechanism is expected.

- The out-of-plane strengthened walls behaved in a bi-linear fashion until rupture of the textile rovings that crossed the mortar joint located at or near mid height (maximum moment point).

- The out-of-plane flexural strength of strengthened walls was observed to range from 5.75 to 7.86 times the strength of the as-built tested wall when the TRM strengthened face of the wall acted in tension. However, the out-of-plane strength was similar to that of the as-built wall when the TRM strengthened face acted in compression.

- Whilst the experimental results show that TRM can increase the strength, ductility, and energy dissipation properties of URM walls, it is noted that the test results are not conclusive in themselves but a step in understanding the performance of TRM strengthened URM walls. Further experimental investigations are warranted to investigate the effect of concurrent in-plane and out-of-plane loading on TRM strengthened URM walls.

5. Acknowledgments

Financial support for the testing reported herein was provided by the New Zealand Foundation for Research Science and Technology. Mapei New Zealand supplied the cement

based TRM systems. Stoanz Limited New Zealand supplied cement free TRM systems and provided financial assistance for this testing. Benoit Rozier, Svend Andersen and Tek Goon Ang are thanked for their help with the testing program.

6. References

[1] Ghobarah A, Saatcioglu M, Nistor I. The impact of the 26 December 2004 earthquake and tsunami on structures and infrastructure. Eng Struct. 2006;28:312-26.

[2] Moon L, Dizhur D, Senaldi I, Derakhshan H, Griffith M, Magenes G et al. The demise of the URM building stock in Christchurch during the 2010-2011 Canterbury earthquake sequence. Earthquake Spectra. 2014;30:253-76.

[3] Tezcan SS, Ipek M. A reconnaissance report: 1995 Dinar, Turkey, earthquake. Eng Struct. 1996;18:906-16.

[4] Zhao B, Taucer F, Rossetto T. Field investigation on the performance of building structures during the 12 May 2008 Wenchuan earthquake in China. Eng Struct. 2009;31:1707-23.

[5] Ismail N, Khattak N. Reconnaissance report on the Mw 7.5 Hindu Kush earthquake of 26th October 2015 and the subsequent aftershocks. Al Ain: United Arab Emirates University; 2015.

[6] Abrams DP. Seismic response patterns for URM buildings. The Masonry Society Journal. 2000;18:71-8.

[7] Magenes G, Calvi GM. In-plane seismic response of brick masonry walls. Earthquake Engineering and Structural Dynamics. 1997;26:1091-112.

[8] Ismail N. Performance of wall to diaphragm anchors for use in seismic upgrade of heritage masonry buildings. International Journal of Architectural Heritage. 2016:In press.

[9] ASCE/SEI. ASCE/SEI 41-13: Seismic rehabilitation of existing buildings. Reston, USA: American Society of Civil Engineers; 2013.

[10] Derakhshan H, Griffith MC, Ingham JM. Airbag testing of multi-leaf unreinforced masonry walls subjected to one-way bending. Eng Struct. 2013;57:512-22.

[11] ACI Committee 440. 440.7R-10: Guide for design and construction of externally bonded FRP systems for strengthening unreinforced masonry structures. Farmington Hills, USA: American Concrete Institute; 2010.

[12] ACI Committee 440. 440.2R-08: Guide for the design and construction of externally bonded FRP systems for strengthening concrete structures. Farmington Hills, USA: American Concrete Institute; 2008.

[13] Triantafillou T. Strengthening of masonry structures using epoxy-bonded FRP laminates. Journal of Composites for Construction. 1998;2:96–104.

[14] Dias SJE, Barros JAO. Performance of reinforced concrete T beams strengthened in shear with NSM CFRP laminates. Eng Struct. 2010;32:373-84.

[15] Dizhur D, Griffith M, Ingham J. Out-of-plane strengthening of unreinforced masonry walls using near surface mounted fibre reinforced polymer strips. Eng Struct. 2014;59:330-43.

[16] ACI Committee 549. ACI 549.4R-13: Guide to design and construction of externally

bonded fabric-reinforced cementitious matrix (FRCM) systems for repair and strengthening concrete and masonry structures. Farmington Hills, USA: American Concrete Institute; 2013.

[17] Bisby L, Stratford T, Smith J, Halpin S. FRP versus fiber reinforced cementitious mortar systems at elevated temperature. 10th International Symposium on Fiber Reinforced Polymer Reinforcement for Concrete Structures. Tampa, USA: ACI Special Publication 275 SP, American Concrete Institute; 2011. p. 863-81.

[18] Triantafillou TC, Papanicolaou CG. Shear strengthening of reinforced concrete members with textile reinforced mortar (TRM) jackets. Materials and Structures/Materiaux et Constructions. 2006;39:93-103.

[19] D'Ambrisi A, Focacci F. Flexural strengthening of RC beams with cement-based composites. Journal of Composites for Construction. 2011;15:707-20.

[20] Loreto G, Leardini L, Arboleda D, Nanni A. Performance of RC slab-type elements strengthened with fabric-reinforced cementitious-matrix composites. Journal of Composites for Construction. 2014;18.

[21] Ombres L. Structural performances of reinforced concrete beams strengthened in shear with a cement based fiber composite material. Composite Structures. 2015;122:316-29.

[22] Babaeidarabad S, De Caso F, Nanni A. URM walls strengthened with fabric-reinforced cementitious matrix composite subjected to diagonal compression. Journal of Composites for Construction. 2014;18.

[23] Faella C, Martinelli E, Nigro E, Paciello S. Shear capacity of masonry walls externally

strengthened by a cement-based composite material: An experimental campaign. Construction and Building Materials. 2010;24:84-93.

[24] Ismail N, Ingham JM. Polymer textiles as a retrofit material for masonry walls. Structures and Buildings. 2014;167:15-25.

[25] Papanicolaou C, Triantafillou T, Lekka M. Externally bonded grids as strengthening and seismic retrofitting materials of masonry panels. Construction and Building Materials. 2011;25:504-14.

[26] Almeida JAPP, Pereira EB, Barros JAO. Assessment of overlay masonry strengthening system under in-plane monotonic and cyclic loading using the diagonal tensile test. Construction and Building Materials. 2015;94:851-65.

[27] Yi T, Moon FL, Leon RT, Kahn LF. Lateral load tests on a two-story unreinforced masonry building. J Struct Eng. 2006;132:652-8.

[28] Foraboschi P. Coupling effect between masonry spandrels and piers. Materials and Structures/Materiaux et Constructions. 2009;42:279-300.

[29] Beyer K. Peak and residual strengths of brick masonry spandrels. Eng Struct. 2012;41:533-47.

[30] Beyer K, Dazio A. Quasi-static cyclic tests on masonry spandrels. Earthquake Spectra. 2012;28:907-29.

[31] Augenti N, Parisi F, Prota A, Manfredi G. Inplane lateral response of a fullscale masonry

subassemblage with and without an inorganic matrixgrid strengthening system. Journal of Composites for Construction. 2011;15:578-90.

[32] Parisi F, Lignola GP, Augenti N, Prota A, Manfredi G. Nonlinear behavior of a masonry subassemblage before and after strengthening with inorganic matrix-grid composites. Journal of Composites for Construction. 2011;15:821-32.

[33] Papanicolaou CG, Triantafillou TC, Papathanasiou M, Karlos K. Textile reinforced mortar (TRM) versus FRP as strengthening material of URM walls: Out-of-plane cyclic loading. Materials and Structures/Materiaux et Constructions. 2008;41:143-57.

[34] Harajli M, ElKhatib H, San-Jose JT. Static and cyclic out-of-plane response of masonry walls strengthened using textile-mortar system. Journal of Materials in Civil Engineering. 2010;22:1171-80.

[35] Babaeidarabad S, Caso FD, Nanni A. Out-of-plane behavior of URM walls strengthened with fabric-reinforced cementitious matrix composite. Journal of Composites for Construction. 2014;18.

[36] Lumantarna R, Biggs DT, Ingham JM. Compressive, flexural bond, and shear bond strengths of in situ New Zealand unreinforced clay brick masonry constructed using lime mortar between the 1880s and 1940s. Journal of Materials in Civil Engineering. 2014;26:559-66.

[37] ASTM. ASTM C1072-10: Standard test method for measurement of masonry flexural bond strength. West Conshohoken, USA: American Society for Testing and Materials International; 2010.

[38] ASTM. ASTM C109 / C109M-11: Standard test method for compressive strength of hydraulic cement mortars. West Conshohoken, USA: American Society for Testing and Materials International; 2011.

[39] ASTM. ASTM C67-11: Standard test methods for sampling and testing brick and structural clay tile. West Conshohoken, USA: American Society for Testing and Materials International; 2011.

[40] ASTM. ASTM C1314-11: Standard test method for compressive strength of masonry prisms. West Conshohoken, USA: American Society for Testing and Materials International; 2011.

[41] ASTM. ASTM E519 / E519M-10: Standard test method for diagonal tension (shear) in masonry assemblages. West Conshohoken, USA: American Society for Testing and Materials International; 2010.

[42] ASTM. ASTM C321-00: Standard test method for bond strength of chemical-resistant mortars. West Conshohoken, USA: American Society for Testing and Materials International; 2000.

[43] ASTM. ASTM D7269-11: Standard test method for tensile testing of Aramid yarns. West Conshohoken, USA: American Society for Testing and Materials International; 2011.

[44] Ismail N, Ingham JM. In-situ and laboratory based out-of-plane testing of unreinforced clay brick masonry walls strengthened using near surface mounted twisted steel bars. Construction and Building Materials. 2013;36:119-28.

[45] Ismail N, Ingham JM. Cyclic out-of-plane behavior of slender clay brick masonry walls seismically strengthened using posttensioning. Journal of Structural Engineering (United States). 2013;138:1255-66.

[46] CEN. Eurocode 8: Design of structures for earthquake resistance. Brussels, Belgium: Comite Europeen de Normalisation (European Committee for Standardization); 2005.

[47] Chopra AK. Dynamics of structures: Theory and applications to earthquake engineering. 3rd ed. Upper Saddle River, USA: Prentice Hall; 2007.

Table 1. Series 1 test wall details

Test Series	Test Wall	Type of loading	Wall dimensions			Strengthening details			
			H (mm)	B (mm)	T (mm)	Grid type	Adhesive mortar	Additional base coat	No. of faces strengthened
1	ABI-1	IP	see Figure 1a		220	-	-	-	-
1	TMI-2	IP	see Figure 1a		220	FG225	RM2	-	1
1	TMI-3	IP	see Figure 1a		220	EF335	RM3	LM1+SM156	1
2	ABO-4	OOP	3670	1200	220	-	-	-	-
2	TMO-5	OOP	3670	1200	220	FG225	RM2	-	1
2	TMO-5′	OOP	3670	1200	220	FG225	RM2	-	1
2	TMO-6	OOP	3670	1200	220	EF335	RM3	LM1+SM156	1
2	TMO-6′	OOP	3670	1200	220	EF335	RM3	LM1+SM156	1

Where: H = test wall height; B = test wall length; T = test wall thickness; IP = in-plane; and OOP = out-of-plane.
′Test wall loaded in out-of-plane direction up to destruction

Table 2. Masonry material properties

Test Series	f'_b (CoV) MPa	f'_j (CoV) MPa	f'_m (CoV) MPa	f_r (CoV) MPa
1	39.4 (0.39)	1.3 (0.26)	10.7 (0.33)	0.09 (0.66)
2	21.3 (0.28)	1.4 (0.18)	6.5 (0.30)	0.08 (0.80)

Where: f'_b = brick compressive strength; f'_j = mortar compressive strength; f'_m = masonry compressive strength; and f_r = flexural bond strength of masonry.

Table 3. Retrofit material properties

Textile	**A_f mm^2/m**	**F_{fu} kN/m**	**E_f GPa**	**Mortar**	**γ_m kN/m^3**	**f_{ma} MPa**
-	-	-	-	-	-	-
FG225	35.27	45	72	LM1	15.4	1.1
EF335	38.68	57	71	RM1	17.6	1.2
SM156	15.70	20	193	RM2	15.7	2.0

Where: A_f = area of polymer fibres; F_{fu} = ultimate tensile strength of polymer grid; E_f = elastic modulus of reinforcement; γ_m = density of cementicious mortar; f_{ma} = mortar adhesion; FG225 = bidirectional Aramid FRP grid weighing 225 gm/m^2; EF335 = bidirectional galls FRP grid weighing 335gm/m^2; SM156 = galvanised steel welded mesh weighing 156 gm/m^2; LM1 = lightweight levelling mortar with polystyrene beads; RM1 = fibre reinforced pozzolonic mortar; and RM2 = mixed polymer dispersion based cementitious mortar.

Table 4. Test results

Test Series	Test wall	Loading direction	V_c kN	V_u kN	K_i kN/m	V_u/V_o Ratio	Δ_c mm	Δ_u mm	γ_u %	μ ratio	ξ %
1	AB-1	+ (Push)	51.6	74.4	12.6	1.0	4.1	24.4	0.9	6.0	5.6
		- (Pull)	-43.7	-75.7	10.4	1.0	-4.2	-24.1	-0.9	5.7	-
1	TMI-2	+ (Push)	62.8	93.7	17.0	1.3	3.7	25.9	1.0	7.0	19.2
		- (Pull)	-52.9	-83.5	12.9	1.1	-4.1	-25.7	-1.0	6.3	-
1	TMI-3	+ (Push)	61.0	101.8	18.5	1.4	3.3	36.8	1.4	11.2	13.7
		- (Pull)	-58.9	-84.7	17.3	1.1	-3.4	-28.9	-1.1	8.5	-
2	ABO-4	+ (Push)	2.6	3.7	0.3	1.0	8.4	56.2	3.1^+	6.7	13.0
		- (Pull)	-3.1	-4.0	0.4	1.0	-8.8	-49.1	-	-	-
2	TMO-5	+ (Push)	15.0	22.2	1.4	6.0	10.4	81.4	4.4^+	7.8	19.6
		- (Pull)	-4.6	-5.1	0.5	1.3	-8.9	-97.4	-	-	-
2	TMO-6	+ (Push)	10.9	26.2	0.8	7.1	14.4	90.9	5.0^+	6.3	11.2
		- (Pull)	-4.7	-4.7	0.5	1.2	-9.2	-57.3	-	-	-
2	TMO-5′	+ (Push)	-	20.9	-	5.6	-	89.6	4.9	8.6	10.8
2	TMO-6′	+ (Push)	-	28.6	-	7.7	-	101.1	5.5	9.2	11.0

Where: V_c = measured lateral force at first cracking; Δ_c = measured displacement at first cracking; V_u = maximum measured lateral force; Δ_u = measured displacement at ultimate limit state; K_i = measured initial stiffness; V_o = strength of as-built tested wall; γ_u = measured story drift at ultimate limit state; μ = pseudo-ductility; and ξ = damping coefficient for the first cycle.

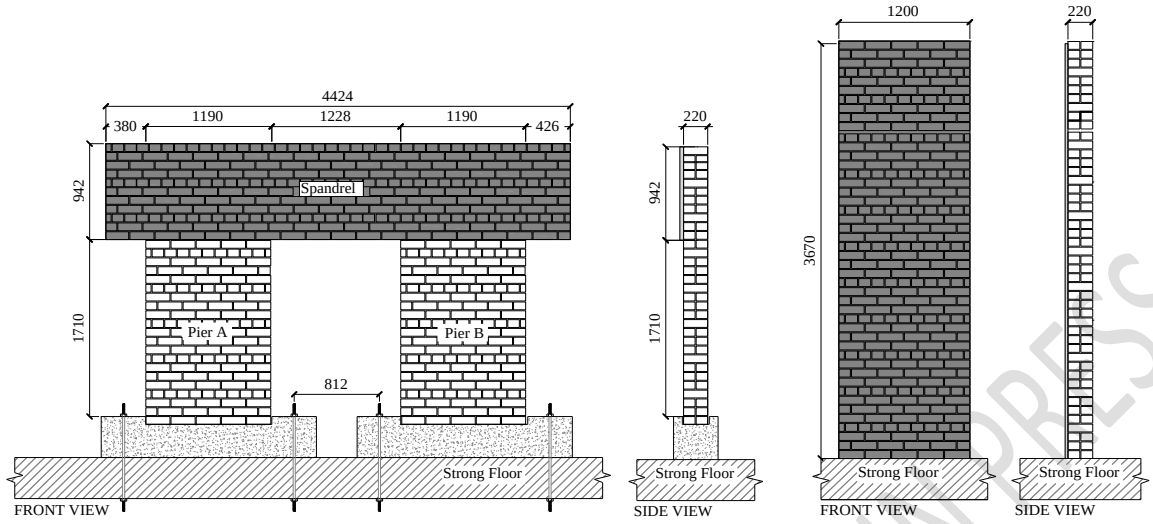

(a) series 1 (b) series 2

Figure 1. Test wall geometric configuration

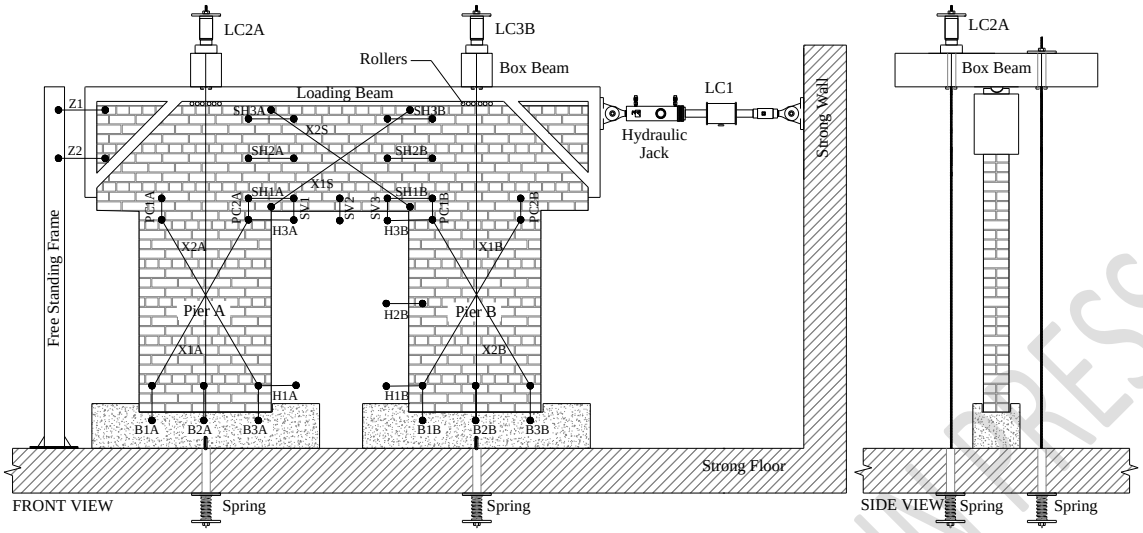

Figure 2. Series 1 test setup

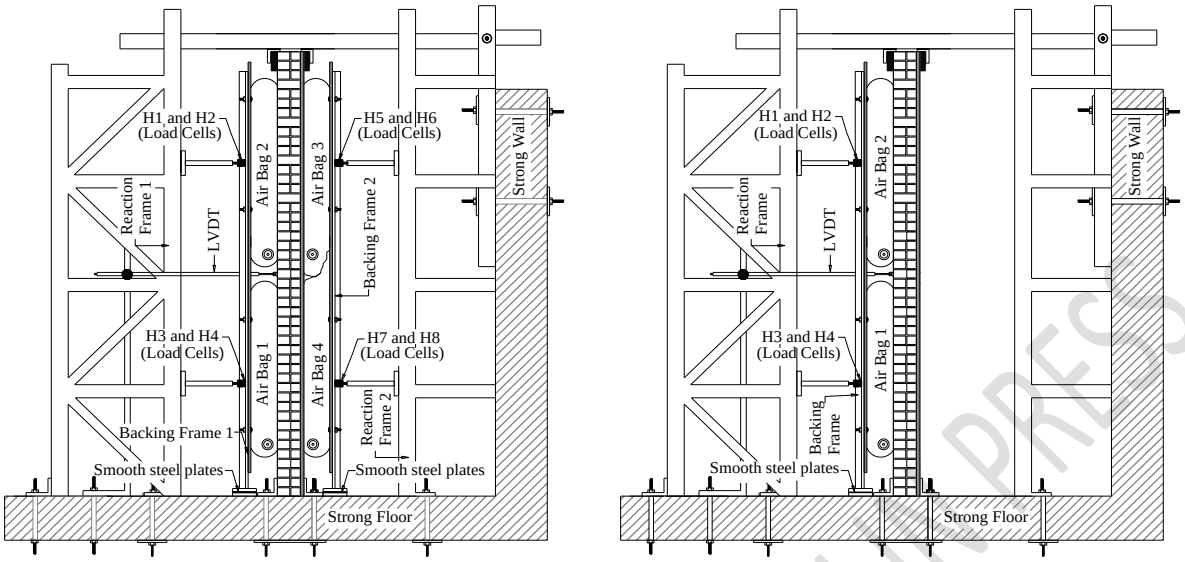

(a) reversed cycling testing (b) one directional cyclic testing

Figure 3. Series 2 test setup

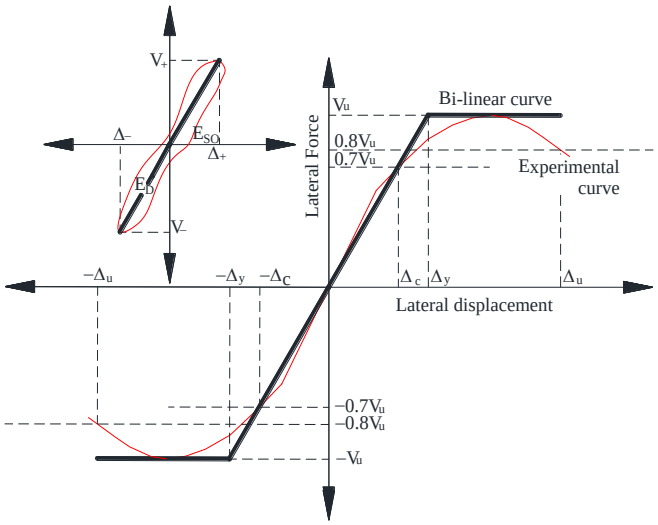

Figure 4. Notations and definition of the adopted elasto-plastic model

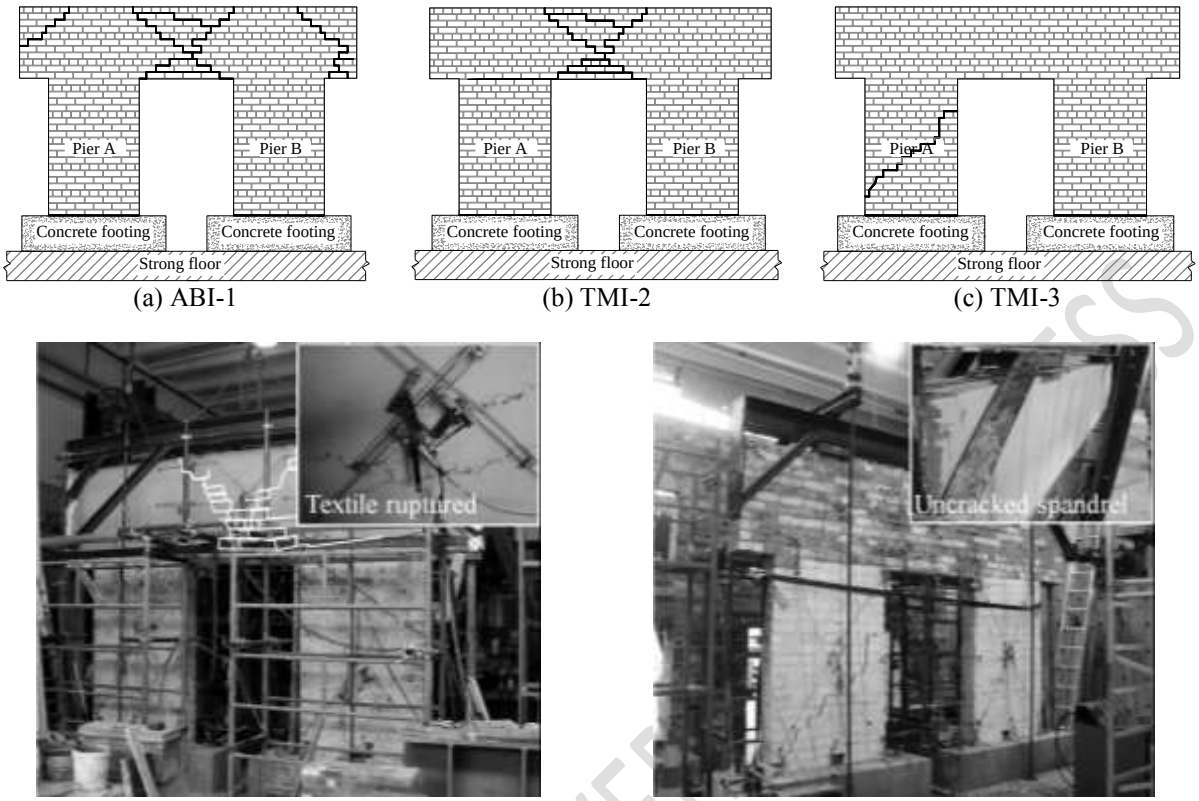

(a) ABI-1 (b) TMI-2 (c) TMI-3

(d) Photograph of TMI-2 (e) Photograph of TMI-3

Figure 5. Damage patterns (series 1)

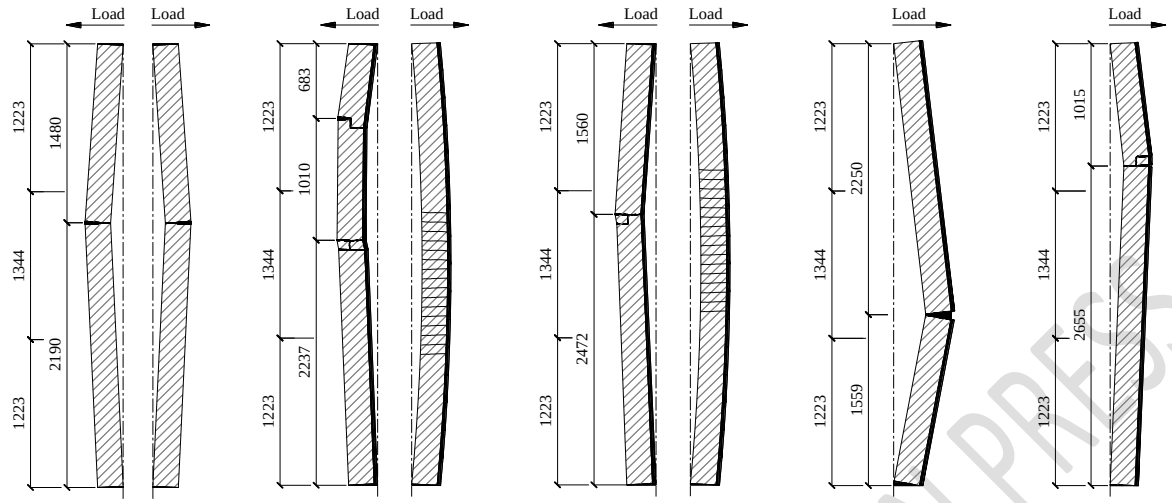

Figure 6. Damage patterns (series 2)

(a) TMO-5′ (b) TMO-6′

Figure 7. Photographs of series 2 test walls at the conclusion of testing

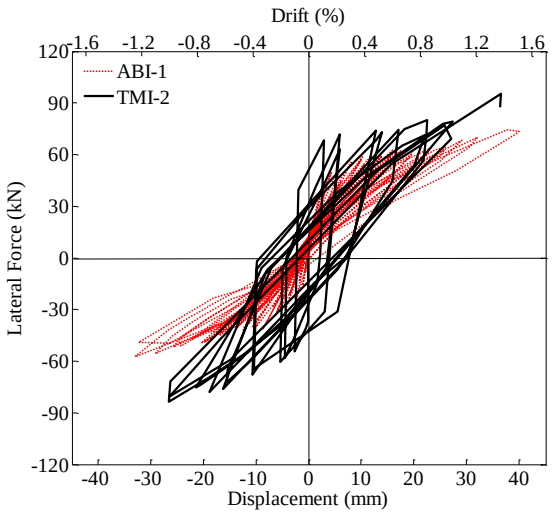

(a) ABI-1 and TMI-2

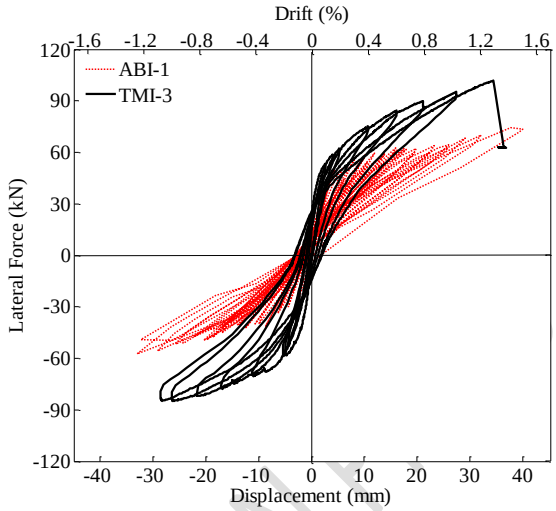

(b) ABI-1 and TMI-3

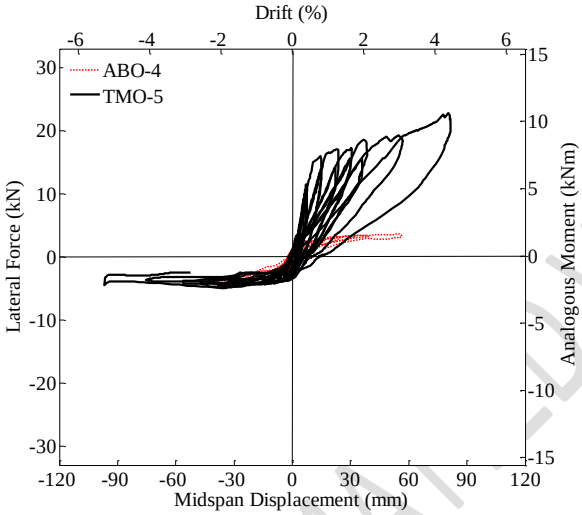

(c) ABO-4 and TMO-5

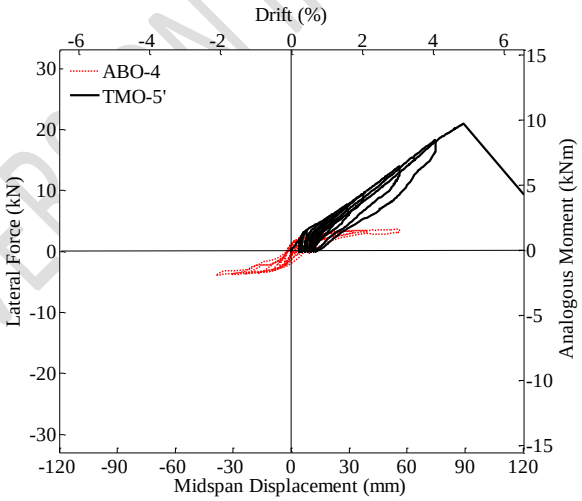

(d) ABO-4 and TMO-5′

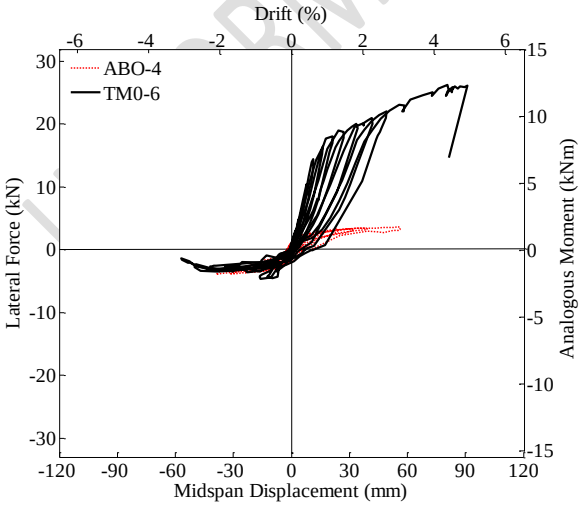

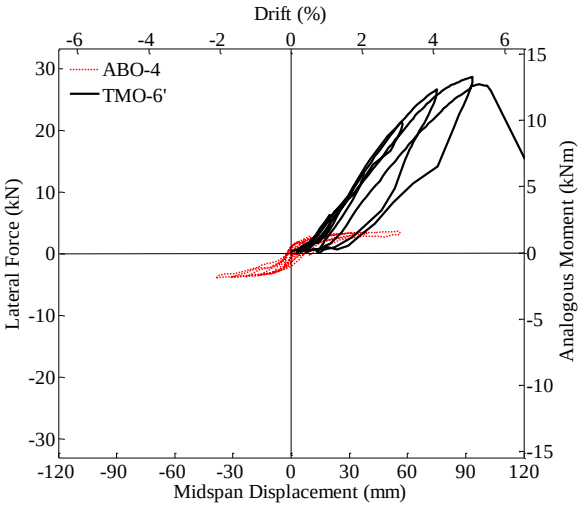

(e) ABO-4 and TMO-6

(f) ABO-4 and TMO-6′

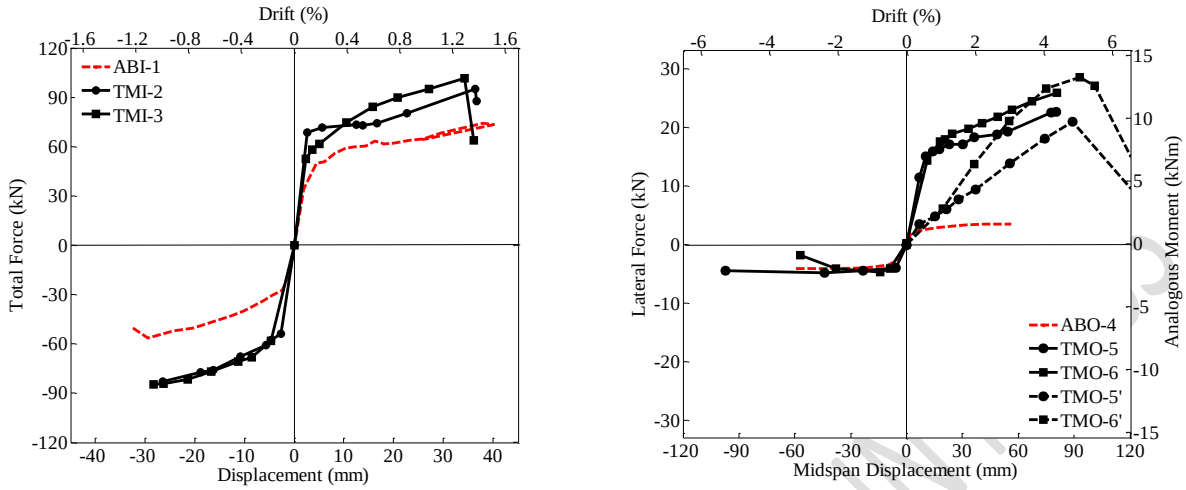

(g) series 1 comparison

(h) series 2 comparison

Figure 8. Experimental hysteretic curves

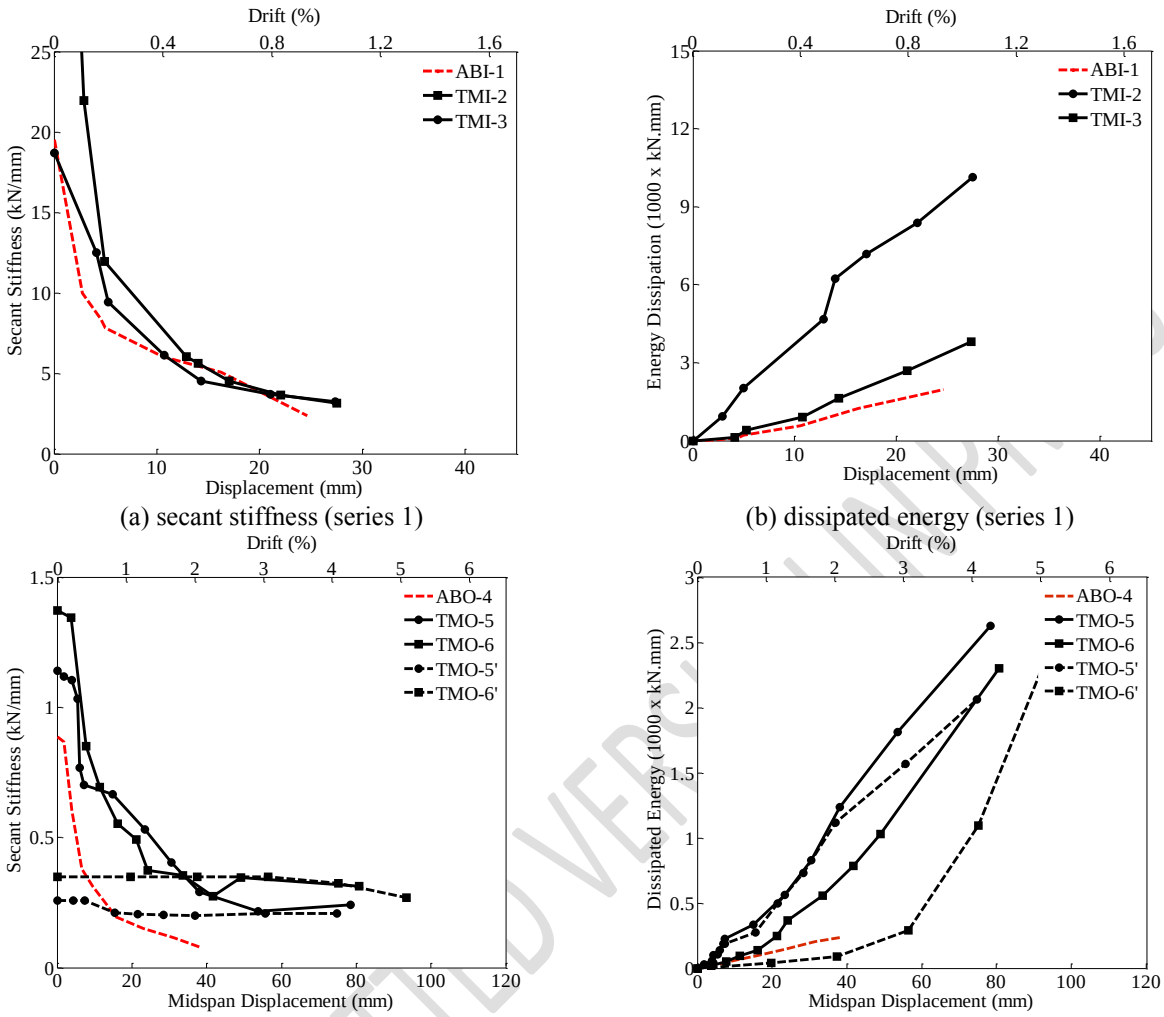

(a) secant stiffness (series 1)

(b) dissipated energy (series 1)

(c) secant stiffness (series 2)

(d) dissipated energy (series 2)

Figure 9. Stiffness degradation and energy dissipation